Cardiac amyloid imaging with ^{18}F-florbetaben positron emission tomography:

a pilot study

W. Phillip Law[1,2], William Y.S. Wang[2,3], Peter T. Moore[3], Peter N. Mollee[2,4], Arnold C.T. Ng [2,3]

[1]Medical Imaging Department, Princess Alexandra Hospital, Brisbane, Australia

[2]School of Medicine, University of Queensland, Brisbane, Australia

[3]Cardiology Department, Princess Alexandra Hospital, Brisbane, Australia

[4]Amyloidosis Centre, Princess Alexandra Hospital, Brisbane, Australia

Address for correspondence:

W. Phillip Law

Medical Imaging Department, Princess Alexandra Hospital

School of Medicine, University of Queensland

Brisbane, Australia 4102

Tel: +61-7-31762144; Fax: +61-7-31762185

Email: phil.law.au@gmail.com

Word count: 4,996 words

ABSTRACT

Aim: Determine the feasibility of ^{18}F-florbetaben positron emission tomography (PET) in diagnosing cardiac amyloidosis. **Methods**: ^{18}F-florbetaben PET was performed in 14 subjects: 5 light chain (AL) amyloid, 5 transthyretin (ATTR) amyloid, and 4 control subjects with hypertensive heart disease. Qualitative and quantitative assessments of ^{18}F-florbetaben activity were performed using mean standardized uptake value (SUV) of the left ventricular (LV) myocardium and blood pool, and calculation of target-to-background SUV ratio. Percentage myocardial ^{18}F-forbetaben retention was also calculated as the percentage mean myocardial SUV change between 0–5mins and 15–20mins after radiotracer injection. Global LV longitudinal and right ventricular (RV) free wall longitudinal strain were calculated using 2D speckle tracking echocardiography. **Results:** Target-to-background SUV ratio and percentage myocardial ^{18}F-forbetaben retention were higher in amyloid patients compared to hypertensive control subjects. A cut-off value of 40% was able to differentiate between cardiac amyloid patients and hypertensive control subjects. Percentage myocardial ^{18}F-forbetaben retention was an independent determinant of both global LV longitudinal and RV free wall longitudinal strain via an inverse curve relationship. **Conclusions**: ^{18}F-florbetaben PET imaging can accurately identify and differentiate between cardiac amyloidosis and hypertensive heart disease. Percentage myocardial ^{18}F-florbetaben retention was an independent determinant of myocardial dysfunction in cardiac amyloidosis.

Keywords: florbetaben; positron emission tomography; amyloidosis; echocardiography

Running title: Florbetaben PET in cardiac amyloidosis

INTRODUCTION

Amyloidosis is a heterogeneous group of disorders that results from the extracellular deposition of insoluble proteins with a unique β-pleated sheet secondary structure, leading to dysfunction of the affected organ (*1*). Although many types of amyloid proteins can deposit in the heart, it is predominantly the AL and senile "wild-type"/hereditary mutant ATTR subtypes that cause clinical cardiac disease. Cardiac amyloidosis is often not diagnosed until late in the course of the disease as the typical appearance of the infiltrated myocardium, impaired LV function, and reduced myocardial Doppler velocities are usually mistaken for other more prevalent causes of concentric LV hypertrophy such as hypertensive heart disease (*1*). By the time clinical manifestation of congestive heart failure is apparent, cardiac amyloidosis portends an extremely poor prognosis and is the main cause of morbidity and mortality. Advanced echocardiographic techniques such as 2-dimensional (2D) speckle tracking strain imaging is useful in demonstrating impaired longitudinal function with apical sparing (*2*). However, it is not pathognomonic for cardiac amyloidosis and cannot differentiate it from other causes of LV hypertrophy with 100% accuracy (*2*).

PET imaging with ^{18}F-labelled florbetaben has been shown to accurately detect β-amyloid neuritic plaques in the brain in patients with Alzheimer's disease (*3*). This agent specifically binds to the amyloid β-pleated sheet structure (*4*). However, its feasibility and accuracy in diagnosing cardiac amyloidosis is unknown. Furthermore, early detection of subclinical cardiac amyloidosis before clinical manifestation of heart failure may permit early initiation of appropriate therapy. Finally, the agent may also permit quantification and monitoring of the burden of amyloid plaque deposition. Therefore, the aims of the present study were to determine the feasibility of ^{18}F-flobetaben PET imaging in diagnosing cardiac

amyloidosis compared to a control group of patients with hypertensive heart disease, and to correlate the extent of ^{18}F-florbetaben myocardial retention with biventricular myocardial dysfunction on 2D speckle tracking echocardiography.

METHODS

Patient population and study protocol

Ten patients with cardiac amyloidosis (5 AL and 5 ATTR subtypes) were prospectively recruited to undergo PET imaging and transthoracic echocardiography. All amyloid patients (AL and ATTR) had echocardiographic features consistent with cardiac amyloidosis. All ATTR amyloid patients had endomyocardial biopsy-proven cardiac amyloid and "wild-type" ATTR, otherwise known as senile cardiac amyloidosis. Patients with AL amyloidosis had biopsy from other organs (kidney, bone marrow, prostate, rectum), and met International Society of Amyloidosis consensus criteria for cardiac involvement (5). The subtype of amyloidosis (AL or ATTR) was determined by tandem mass spectrometry in 6 subjects and immunohistochemistry or immunofluorescence in 4 subjects. Genetic testing for transthyretin gene mutations was negative in all ATTR cases.

As per guidelines, echocardiographic definition of cardiac amyloidosis included LV wall thickness >12mm, granular sparkling of the myocardium, RV free wall thickness >5mm, increased atrioventricular valve or interatrial septal thickness, pericardial effusion, and LV diastolic dysfunction (based on mitral inflow, pulmonary venous flow, and tissue Doppler imaging of septal and lateral mitral annulus) (5).

As LV hypertrophy due to hypertensive heart disease is a frequent differential diagnosis for cardiac amyloidosis, 4 hypertensive control subjects with echocardiographic evidence of concentric LV hypertrophy were also prospectively recruited.

None of the subjects had echocardiographic or cardiac magnetic resonance imaging features that would suggest hypertrophic cardiomyopathy or variants.

Laboratory examinations included glomerular filtration rates calculated by the Modification of Diet in Renal Disease formula (6), cardiac troponin-I, and B-type natriuretic peptide (BNP).

Exclusion criteria for all amyloidosis and hypertensive control patients included presence of moderate or severe valvular heart disease, congenital heart disease, severe claustrophobia, pregnancy, and inability to lie flat for 80mins. Additional exclusion criteria for the hypertensive control subjects included previously known congestive cardiac failure, myocardial infarction, and LV ejection fraction <50%.

The study was approved by the institutional ethics committee and all patients provided written informed consent.

Cardiac PET data acquisition

Cardiac PET (Biograph-128 mCT; Siemens, Erlangen, Germany) was performed in list-mode for 80mins. As the distribution of ^{18}F-florbetaben in the heart has not been previously reported, a long scan acquisition time was required to enable selection of optimal imaging protocol for future studies. Low-dose computed tomography (CT) (tube current 40mA.s, tube voltage 120kV) was performed through the heart during tidal respiration for attenuation correction and to aid in anatomical localization of radiotracer activity. PET acquisition was

commenced at the same time as the intravenous injection of 4MBq/kg (0.1mCi/kg) of ^{18}F-florbetaben for each subject, administered as a single intravenous bolus without any observed haemodynamic effects. The average activity received by the subjects was 259MBq (7mCi) [SD, 41MBq (1.1mCi)]. Dynamic images were reconstructed from the list-mode data using 80 frames of 1min each, with a matrix size of 200 x 200, employing an ordered subset expectation maximization iterative reconstruction technique (3 iterations, 21 subsets). Static images were reconstructed with a matrix size of 400 x 400 and a slice thickness of 3mm. The estimated whole-body effective radiation dose to each subject was 5.8mSv.

Cardiac PET analyses

Qualitative visual assessment of myocardial ^{18}F-florbetaben uptake was performed using static images reconstructed from PET data acquired between 15–75mins after the injection of ^{18}F-florbetaben. To further assess the image contrast between myocardial ^{18}F-florbetaben uptake against the background blood pool over time (hereby defined as the target-to-background ratio), mean SUV in LV myocardium and the blood pool were plotted every minute and displayed graphically. Therefore, a higher target-to-background ratio is represented by a greater curve separation between myocardial SUV and the background blood pool SUV over time. LV myocardial SUV was calculated by placing a volume-of-interest around the heart on summed images between 5–10mins post-radiotracer injection, when there was maximal difference between myocardial and ventricular luminal blood pool SUV (Fig. 1). Using a commercially available software-automated isocontour function (*syngo.via*, Siemens Healthcare, Germany), the obtained myocardial contour was transposed to the remainder of the frames for dynamic analysis (Supplemental Fig. 1). The default isocontour threshold of 40% SUVmax was used as this

corresponded best with the actual boundaries of the myocardium, as is the case generally with tumour imaging with PET as recommended by guidelines (7). Blood pool SUV was measured using a region of interest of 1cm diameter in the mid-descending thoracic aorta (extended over 2cm in the z-axis) that can also be generated as an automated function in the software used for PET analysis and provides the benefits of reproducibility, ease of performance, and accuracy of localisation of blood pool activity.

To quantify myocardial accumulation of ^{18}F-florbetaben, both ^{18}F-florbetaben retention index (RI) and percentage myocardial ^{18}F-florbetaben retention were calculated. ^{18}F-florbetaben RI was calculated as the mean myocardial ^{18}F-florbetaben SUV between 15–20mins after injection divided by the integral of the arterial time-activity curve between 0–17.5mins after injection, the midpoint of 15–20mins (8). Percentage myocardial ^{18}F-florbetaben retention was calculated based on the change in mean SUV on summed-framed images of the LV myocardium between 0–5mins and 15–20mins following radiotracer injection using the formula:

Percentage myocardial ^{18}F-florbetaben retention $= \left[1 - \left(\frac{SUV_{0-5} - SUV_{15-20}}{SUV_{0-5}}\right)\right] \times 100\%$

where SUV_{0-5} = mean myocardial SUV between 0–5mins; SUV_{15-20} = mean myocardial SUV between 15–20mins.

Echocardiography

Transthoracic echocardiography was performed with the subjects at rest using a commercially available ultrasound system (Vivid E9, 4V probe, GE-Vingmed, Horten, Norway) and digitally stored for offline analysis (EchoPAC version 113, GE-Vingmed, Horten, Norway). A complete 2D, colour, pulsed and continuous-wave Doppler echocardiogram was performed according to standard techniques (9,10).

LV mass index was calculated[7] and corrected for body surface area (*11*). Relative wall thickness was calculated (*10*). LV end-diastolic volume index and end-systolic volume index were calculated using Simpson's biplane method of discs and corrected for body surface area. LV ejection fraction was derived. Stroke volume was calculated from LV outflow tract cross-sectional area and the velocity-time-integral, and indexed to body surface area. Cardiac output was derived from the calculated stroke volume and heart rate.

RV free wall thickness was measured at the level of the tricuspid annulus in the 2D subcostal view (*12*). RV end-diastolic area, end-systolic area and fractional area change were measured (*12*).

Mitral inflow early (E wave) and late (A wave) diastolic velocities, and pulmonary venous peak systolic and diastolic velocities were recorded using pulsed-wave Doppler echocardiography in the apical 4 chamber view.

Pulsed-wave tissue Doppler velocities were recorded at the septal and lateral mitral annulus in the apical 4 chamber view mitral annular systolic (s') and early diastolic (e') velocities were obtained (*13*). LV filling pressure (E/e') was calculated as the ratio of transmitral E wave to average mitral annular e' velocity. Tricuspid annular s' and e' velocities were also recorded.

2D speckle tracking analyses were performed on standard grey scale images in the apical 2-, 3- and 4-chamber views. LV global longitudinal strain was calculated from the 3 individual apical global longitudinal strain curves, whereas RV free wall longitudinal strain was obtained from the apical 4-chamber view (*13*).

All PET analyses were performed blinded to the echocardiographic results. As the PET analyses were automated, there were no intra- or interobserver measurement variabilities for myocardial SUV, background blood pool SUV and myocardial ^{18}F-florbetaben RI. All echocardiographic analyses were also performed blinded to the PET results. Previous work has reported the intra- and interobserver measurement variabilities for longitudinal strain of 1.2±0.5% and 0.9±1.0% respectively expressed as mean absolute difference (14). Using a similar methodology, the intra- and interobserver variabilities for measurement of global longitudinal strain in the present study was 0.8±0.3% and 1.0±0.5% respectively expressed as mean absolute difference ± 1 standard deviation.

Statistical analysis

Continuous variables were presented as mean ± 1 standard deviation, and categorical variables were presented as frequencies and percentages. When comparing categorical variables, the exact chi-square test using the Monte Carlo method with 99% confidence interval and 10 000 sample number was used to calculate the p value. The Kruskal-Wallis test was used to compare 3 groups of continuous variables, and Mann-Whitney U test was used to compare 2 groups of continuous variables. For significant results, post-hoc multiple comparisons were performed using Bonferroni corrections. Pearson correlation was used to determine the association between 2 continuous variables. To determine the correlation between myocardial ^{18}F-florbetaben RI and biventricular strain, myocardial ^{18}F-florbetaben RI was first inverse transformed. Multiple linear regression analyses were then used to determine the independent association between the inverse transformed myocardial ^{18}F-florbetaben RI and global LV/RV free wall longitudinal strain. To prevent over-fitting of the data, only a maximum of 2 of the most significant univariable

predictors were sequentially entered into the multiple linear regression models. In addition, a tolerance of <0.5 (equating to R value >0.7) was set to avoid multicolinearity. To determine the relative contribution of each predictor in the multivariable analyses, standardized β values were presented. A 2-tailed p value of <0.05 was considered significant. All statistical analyses were performed using IBM SPSS Statistics for Windows, version 22.0 (Armonk, NY).

RESULTS

Baseline clinical, echocardiographic and PET characteristics of all the subjects are presented in Supplemental Table 1. There were no significant differences in age and body mass index between the 3 groups of patients, and there was a trend towards lower renal function in amyloid patients.

Amyloid patients had significantly higher relative wall thickness than the hypertensive controls, but there was no significant difference in LV mass index between the 3 groups. Although there were no differences in indexed LV volumes and LV ejection fraction, amyloid patients had significantly lower stroke volume index and cardiac index. On tissue Doppler imaging, amyloid patients had significantly lower myocardial systolic and early diastolic velocities, and higher LV filling pressures compared to hypertensive controls.

PET qualitative image assessment

The overall quality of ^{18}F-florbetaben PET static images was excellent in all subjects. Diffusely increased myocardial radiotracer uptake was observed in all AL and ATTR patients, and none in the hypertensive control subjects (Fig. 2). All amyloid patients and hypertensive control subjects showed intense ^{18}F-florbetaben uptake in the liver and imaged bowel loops in

keeping with hepatobiliary excretion of ^{18}F-florbetaben. This did not interfere with the visualisation of myocardial ^{18}F-florbetaben uptake. ^{18}F-florbetaben uptake was also seen in the skeleton – particularly the vertebrae and to a lesser extent the ribs and sternum – the mechanism and significance of which were uncertain.

^{18}F-florbetaben target-to-background ratio

Quantitative assessment myocardial ^{18}F-florbetaben uptake against the background blood pool was performed in all 3 groups of patients and shown in Fig. 3.

Peak blood pool ^{18}F-florbetaben activity was observed in the first 2mins of injection in all amyloid and hypertensive control subjects, while peak LV myocardial ^{18}F-florbetaben activity occurred at the same time or slightly (within 1min) later than peak blood pool activity (Fig. 3). In both AL and ATTR amyloid patients, there were significantly higher target-to-background ratios compared to the hypertensive control subjects from about 10mins after radiotracer injection, which persisted until the end of image acquisition at 80mins (Figs. 2 and 3).

AL amyloid patients had higher target-to-background ratio compared to ATTR amyloid patients as represented by the greater myocardial versus background blood pool SUV curve separation throughout the entire image acquisition duration (Fig. 3). However, AL amyloid patients had significantly higher myocardial ^{18}F-florbetaben SUV variability compared to ATTR amyloid patients.

The blood pool SUV curves showed similar shapes and variabilities for all 3 groups.

Myocardial ^{18}F-florbetaben retention index

Fig. 4 shows the time course of ^{18}F-florbetaben RI for all 3 groups. Fig. 5 shows that the median myocardial ^{18}F-florbetaben RI was 0.043min^{-1} (range, 0.032–0.065min^{-1}) in AL amyloid patients, 0.035min^{-1} (range, 0.022–0.042min^{-1}) in ATTR amyloid patients, and 0.010min^{-1} (range, 0.008–0.015min^{-1}) in hypertensive control subjects. A myocardial RI of >0.020min^{-1} identified all amyloid patients and none of the control subjects (Fig. 5).

Percentage myocardial ^{18}F-florbetaben retention

The median percentage myocardial ^{18}F-florbetaben retention for AL amyloid, ATTR amyloid and hypertensive control subjects were 76.2% (range, 45.3–157.2%), 71.2% (range, 51.3–104.7%) in ATTR subjects, and 28.8% (range, 24.5–35.4%) respectively (p=0.018). There were significant differences in the percentage myocardial ^{18}F-florbetaben retention between AL amyloid patients and hypertensive control subjects (p=0.042 with Bonferroni correction), between ATTR amyloid patients and hypertensive control subjects (p=0.042 with Bonferroni correction), but no difference between AL and ATTR amyloid patients (p>0.99 with Bonferroni correction).

Fig. 6 demonstrates the box plots for the percentage myocardial ^{18}F-florbetaben retention for the 3 groups of patients. There was a clear separation between AL/ATTR amyloid patients and hypertensive control subjects. A cut-off value of >40% was able to differentiate between AL/ATTR amyloid patients and hypertensive control subjects.

Biventricular myocardial contractile function

On 2D speckle tracking, amyloid patients had significantly more impaired LV global longitudinal strain, and a trend towards more impaired RV free wall longitudinal strain. Fig. 7

shows that the relationships between percentage myocardial ^{18}F-florbetaben retention and LV global longitudinal strain and RV free wall longitudinal strain can be expressed by an inverse curve relationship (i.e. $y = a + 1/x$, where a = constant). Therefore, to evaluate the correlation between percentage myocardial ^{18}F-florbetaben retention and biventricular longitudinal strain, the percentage myocardial ^{18}F-florbetaben retention was first inverse transformed. On univariable analyses, the inverse percentage myocardial ^{18}F-florbetaben retention was significantly correlated with LV global longitudinal strain (r=-0.91, p<0.001) and RV free wall longitudinal strain (r=-0.80, p=0.001). Similarly, when the hypertensive control subjects were excluded from the analyses, inverse percentage myocardial ^{18}F-florbetaben retention was still significantly correlated with LV global longitudinal strain (r=-0.84, p=0.003) and RV free wall longitudinal strain (r=-0.74, p=0.015).

There were no correlations between inverse percentage myocardial ^{18}F-florbetaben retention and BNP (r=-0.15, p=0.69), cardiac troponin-I (r=-0.26, p=0.46), interventricular septal wall thickness (r=-0.46, p=0.10), posterior wall thickness (r=-0.53, p=0.054), or LV mass index (r=-0.08, p=0.78). However, inverse percentage myocardial ^{18}F-florbetaben retention was significantly correlated with LV relative wall thickness (r=-0.54, p=0.045) and RV free wall thickness (r=-0.66, p=0.01). When hypertensive control subjects were excluded, there were no correlations between inverse percentage myocardial ^{18}F-florbetaben retention and LV relative wall thickness and RV free wall thickness (all p>0.05).

Supplemental Table 2 outlines the significant univariable determinants of LV global longitudinal strain. There were significant colinearities between systolic blood pressure, diastolic blood pressure, interventricular septal wall thickness and posterior wall thickness. Therefore, only inverse percentage myocardial ^{18}F-florbetaben retention and posterior wall thickness were

sequentially entered into the multiple linear regression model. On multivariable analysis, inverse percentage myocardial ^{18}F-florbetaben retention was the only and most significant independent determinant of LV global longitudinal strain (standardized β=-0.804, p<0.001; model R=0.929). Similar results were obtained when hypertensive control subjects were excluded from the analysis (standardized β=-0.845, p=0.002; model R=0.893). In addition, similar multivariable analysis results were obtained using inverse ^{18}F-florbetaben RI (standardized β=-0.725, p=0.001; model R=0.877).

Supplemental Table 2 also depicts the significant univariable determinants of RV free wall longitudinal strain. There was significant colinearity between RV free wall thickness and interventricular septal wall thickness. Therefore, only inverse percentage myocardial ^{18}F-florbetaben retention and RV free wall thickness were sequentially entered into the multiple linear regression model. On multivariable analysis, only inverse percentage myocardial ^{18}F-florbetaben retention was an independent determinant of RV free wall longitudinal strain (standardized β=-0.607, p=0.021; model R=0.829). Likewise, when hypertensive control subjects were excluded from the analysis, inverse percentage myocardial ^{18}F-florbetaben retention was still an independent determinant of RV free wall longitudinal strain (standardized β=-0.686, p=0.024).

DISCUSSION

The present study demonstrated that ^{18}F-florbetaben PET can accurately identify cardiac amyloidosis and appears promising for the differentiation of myocardial thickening secondary to amyloid deposition from hypertensive heart disease. Furthermore, there was an inverse curve relationship between percentage myocardial ^{18}F-florbetaben retention and biventricular

myocardial contractile function. However, based on the current protocol, ^{18}F-florbetaben PET cannot readily differentiate between AL and ATTR amyloid subtypes.

[18]F-florbetaben PET imaging and diagnosis of cardiac amyloidosis

In a recent pilot study, Dorbala and co-workers showed that ^{18}F-florbetapir can accurately identify cardiac amyloidosis patients from normal healthy control subjects (*15*). However, the main diagnostic dilemma for a patient with cardiac amyloidosis is differentiating it from other more common causes of LV hypertrophy such as hypertensive heart disease (*16*). As cardiac amyloidosis confers a significantly worse long term prognosis, diagnosis requires a plethora of tests including physical examination, cardiac troponin, BNP, electrocardiogram, echocardiogram, and cardiac magnetic resonance imaging (MRI) (*16*). Although results of these tests may be suggestive of cardiac amyloidosis, no single finding is pathognomonic of the disease. Consequently, an invasive endomyocardial biopsy may often be required, especially when common coexisting cardiac diseases such as severe hypertensive or aortic stenosis that cause LV hypertrophy is present (*16*). Therefore, developing a new non-invasive diagnostic test for cardiac amyloidosis demands high sensitivity and specificity. One of the major strengths of the present study was the inclusion of the hypertensive controls with evidence of LV hypertrophy on echocardiography. ^{18}F-florbetaben appears promising for the differentiation of cardiac amyloidosis from hypertensive heart disease. Future studies investigating ^{18}F-florbetaben uptake pattern in other (non-amyloid, non-hypertensive) causes of myocardial thickening would further clarify the specificity of ^{18}F-florbetaben.

[18]F-florbetaben PET imaging also offers additional advantages compared to cardiac MRI. Although cardiac MRI has an established role in diagnosing cardiac amyloidosis, from patterns

of delayed enhancement to T1 mapping for increased interstitial space (*16-18*), patients often have coexisting renal dysfunction that prevents the use of intravenous gadolinium. Furthermore, MRI incompatible devices such as pacemakers will limit the role of cardiac MRI. Finally, unlike ^{18}F-florbetaben that specifically binds to amyloid plaques, diagnosis of cardiac amyloidosis by MRI frequently depends on patterns late gadolinium enhancement. As such, a recent study reported a >5% false positive rate in cardiac MRI based on late gadolinium enhancement (*18*).

It will also be interesting to see if measurements of clinical disease activity such as troponin I and BNP as well as free light chains and TTR circulating levels correlate with ^{18}F-florbetaben retention in larger patient cohorts, as the small subject numbers in the present study would not be expected to show a significant correlation even if one truly existed.

Myocardial ^{18}F-florbetaben retention and biventricular contractile function

Beyond just diagnosing cardiac amyloid involvement with high accuracy, ^{18}F-florbetaben PET may have a role in monitoring amyloid plaque burden and correlate it with the extent of myocardial dysfunction, potentially as part of assessing response to therapy. The present study is the first to demonstrate that percentage myocardial ^{18}F-florbetaben retention was significantly correlated with biventricular contractile function via an inverse curve relationship (Fig. 7). Thus, small initial increases in myocardial ^{18}F-florbetaben RI result in rapid deterioration in myocardial contractile function. Therefore, this suggests that early detection and treatment of cardiac amyloidosis is important to prevent disproportionate and potentially irreversible myocardial dysfunction. Future studies with larger sample size are required to confirm the interpretative significance of the multivariate analysis.

Although there was no significant difference between percentage myocardial ^{18}F-florbetaben retention for AL and ATTR amyloid subtypes, there was significantly higher myocardial SUV variability for AL amyloid patients (Fig. 3). It is unclear if this observation was indicative of greater variability in amyloid plaque burden in AL amyloid patients as these patients did not undergo endomyocardial biopsies for quantification of amyloid plaque burden. However, a recent MRI study demonstrated that ATTR amyloid patients had concomitant cellular hypertrophy in addition to increased extracellular volume compared to AL amyloid patients (19). Therefore, in the present study whereby AL and ATTR amyloid patients had comparative LV mass indexes, it is likely that the AL amyloid patients had correspondingly larger extracellular volume and more amyloid deposition compared to the ATTR amyloid patients, consequently reflected in a higher myocardial SUV. This supports the hypothesis that, due to the slower pace of amyloid accumulation, patients with ATTR have time to develop compensatory ventricular muscle hypertrophy and may explain why patients with AL have more rapidly progressive heart failure and worse survival compared to ATTR in spite of relatively less LV mass (20).

CONCLUSIONS

In this pilot study that included a selected cohort of amyloid and hypertensive control subjects, ^{18}F-florbetaben appears promising for the identification of cardiac amyloidosis, and percentage myocardial ^{18}F-florbetaben retention was correlated with the extent of biventricular myocardial dysfunction. These are, however, preliminary findings based on a small number of subjects and while encouraging require validation in larger populations with a greater heterogeneity of both amyloid patients and patients with non-amyloid myocardial thickening.

Future studies should also include patients with early disease who are yet to fulfil diagnostic criteria for cardiac amyloidosis, correlate percentage myocardial ^{18}F-florbetaben retention with histological amyloid plaque burden, and determine the feasibility ^{18}F-florbetaben PET in monitoring response to therapy. Tailored molecular imaging with PET using ^{18}F-florbetaben may significantly simplify the diagnostic algorithm for cardiac amyloidosis.

REFERENCES

(*1*) Falk RH, Dubrey SW. Amyloid heart disease. *Prog Cardiovasc Dis*. 2010;52:347-361.

(*2*) Phelan D, Collier P, Thavendiranathan P, et al. Relative apical sparing of longitudinal strain using two-dimensional speckle-tracking echocardiography is both sensitive and specific for the diagnosis of cardiac amyloidosis. *Heart*. 2012;98:1442-1448.

(*3*) Villemagne VL, Ong K, Mulligan RS, et al. Amyloid imaging with (18)F-florbetaben in Alzheimer disease and other dementias. *J Nucl Med*. 2011;52:1210-1217.

(*4*) Frisoni GB. PET and 18F ligands in the diagnosis of Alzheimer's disease. *Lancet Neurol*. 2011;10:397-399.

(*5*) Gertz MA, Comenzo R, Falk RH, et al. Definition of organ involvement and treatment response in immunoglobulin light chain amyloidosis (AL): a consensus opinion from the 10th International Symposium on Amyloid and Amyloidosis, Tours, France, 18-22 April 2004. *Am J Hematol*. 2005;79:319-328.

(*6*) National Kidney Foundation Disease Outcomes Quality Initiative. Clinical practice guidelines for chronic kidney disease: evaluation, classification and stratification. *Am J Kidney Dis*. 2002;39:S1-S266.

(*7*) Boellaard R, O'Doherty MJ, Weber WA, et al. FDG PET and PET/CT: EANM procedure guidelines for tumour PET imaging: version 1.0. *Eur J Nucl Med Mol Imaging*. 2010;37:181-200.

(*8*) Antoni G, Lubberink M, Estrada S, et al. In vivo visualization of amyloid deposits in the heart with 11C-PIB and PET. *J Nucl Med*. 2013;54:213-220.

(*9*) Tajik A, Seward J, Hagler D, Mair D, Lie J. Two dimensional real-time ultrasonic imaging of the heart and great vessels: technique, image orientation, structure identification and validation. *Mayo Clin Proc*. 1978;53:271-303.

(*10*) Lang RM, Bierig M, Devereux RB, et al. Recommendations for chamber quantification: a report from the American Society of Echocardiography's Guidelines and Standards Committee and the Chamber Quantification Writing Group, developed in conjunction with the European Association of Echocardiography, a branch of the European Society of Cardiology. *J Am Soc Echocardiogr*. 2005;18:1440-1463.

(*11*) Mosteller RD. Simplified calculation of body-surface area. *N Engl J Med*. 1987;317:1098 (correspondence).

(*12*) Rudski LG, Lai WW, Afilalo J, et al. Guidelines for the echocardiographic assessment of the right heart in adults: a report from the American Society of Echocardiography endorsed by the European Association of Echocardiography, a registered branch of the European Society of Cardiology, and the Canadian Society of Echocardiography. *J Am Soc Echocardiogr*. 2010;23:685-713.

(*13*) Ng AC, Delgado V, Bertini M, et al. Myocardial steatosis and biventricular strain and strain rate imaging in patients with type 2 diabetes mellitus. *Circulation*. 2010;122:2538-2544.

(*14*) Ng ACT, Delgado V, Bertini M, et al. Findings from left ventricular strain and strain rate imaging in asymptomatic patients with type 2 diabetes mellitus. *Am J Cardiol*. 2009;104:1398-1401.

(*15*) Dorbala S, Vangala D, Semer J, et al. Imaging cardiac amyloidosis: a pilot study using ^{18}F-florbetapir positron emission tomography. *Eur J Nucl Med Mol Imaging*. 2014;41:1652-1662.

(*16*) Dubrey SW, Hawkins PN, Falk RH. Amyloid diseases of the heart: assessment, diagnosis, and referral. *Heart*. 2011;97:75-84.

(*17*) Bandula S, Banypersad SM, Sado D, et al. Measurement of tissue interstitial volume in healthy patients and those with amyloidosis with equilibrium contrast-enhanced MR imaging. *Radiology*. 2013;268:858-864.

(*18*) Dungu JN, Valencia O, Pinney JH, et al. CMR-based differentiation of AL and ATTR cardiac amyloidosis. *JACC Cardiovasc Imaging*. 2014;7:133-142.

(*19*) Fontana M, Banypersad SM, Treibel TA, et al. Differential myocyte responses in patients with cardiac transthyretin amyloidosis and light-chain amyloidosis: a cardiac MR imaging study. *Radiology*. 2015;277:388-397.

(*20*) Quarta CC, Solomon SD, Uraizee I, et al. Left ventricular structure and function in transthyretin-related versus light-chain cardiac amyloidosis. *Circulation*. 2014;129:1840-1849.

Fig. 1. Example of software automated volume-of-interest isocontouring performed on 5−10min

post-florbetaben images in a patient with cardiac amyloidosis.
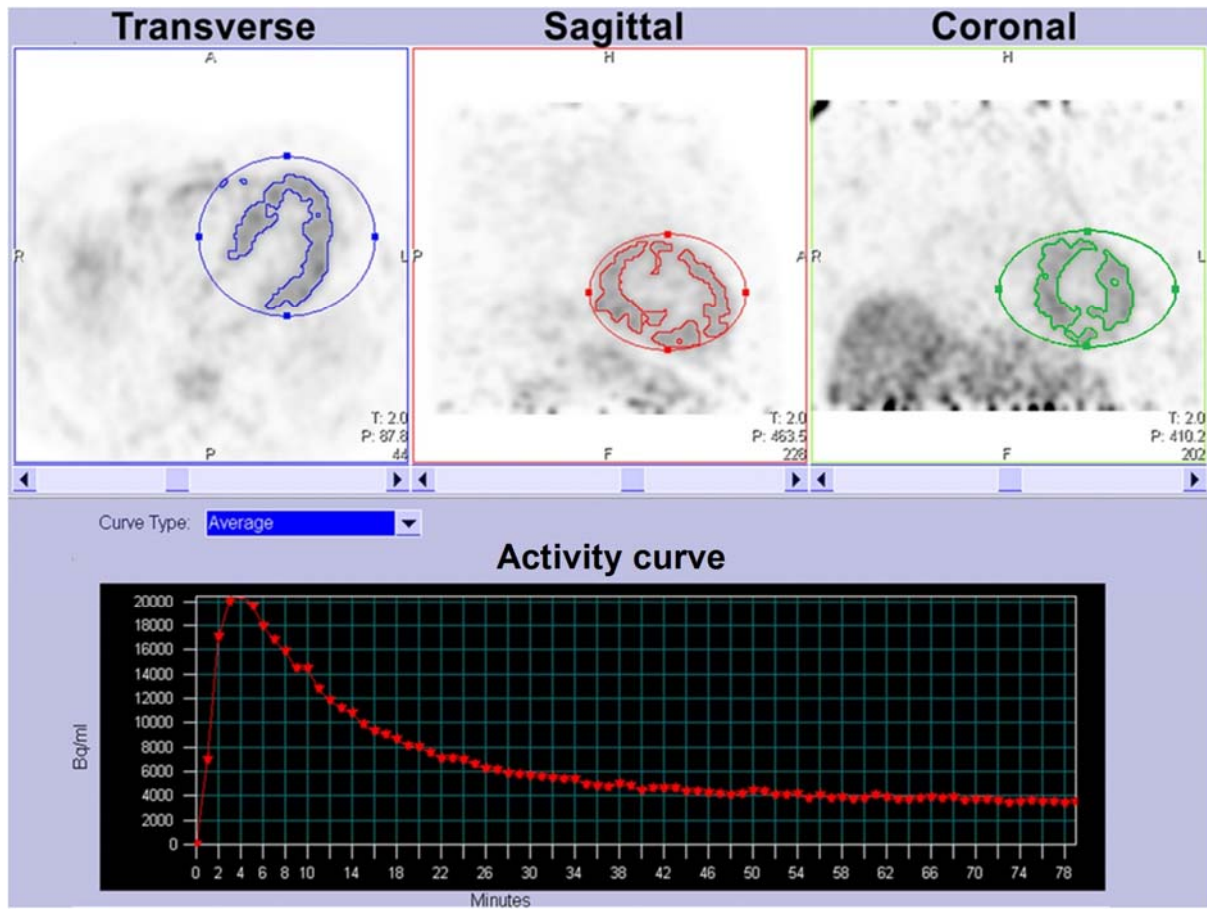
Fig. 2. ^{18}F-Florbetaben PET (left columns in each panel), low-dose CT (middle columns), and fused PET/CT images (right columns) in three representative AL, ATTR and control subjects. There was diffuse avid ^{18}F-florbetaben myocardial uptake in both AL and ATTR amyloid patients, but little radiotracer uptake in the myocardium of the hypertensive control subject. PET images were windowed to display myocardial boundaries.
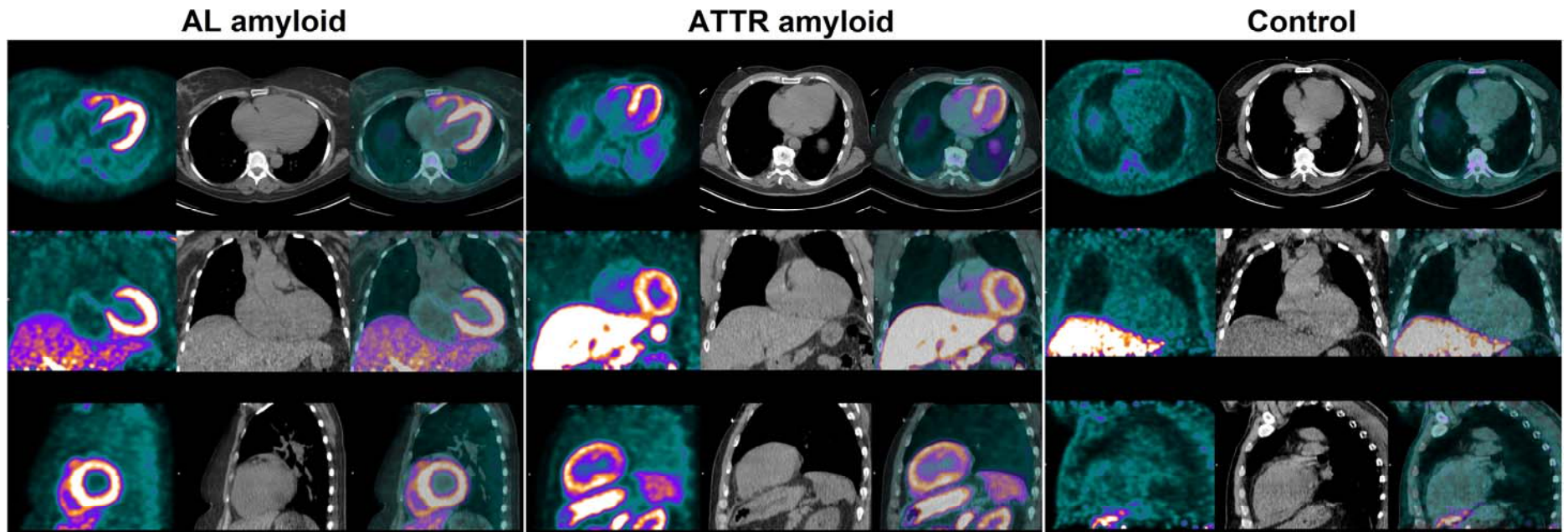
Fig. 3. ^{18}F-Florbetaben time-activity curves in AL, ATTR and control subjects. Mean SUVs in LV myocardium and blood pool peak at 2−3mins after radiotracer injection. After the initial 10mins, there were significantly higher target-to-background ratios in AL and ATTR subjects compared with hypertensive control subjects which persisted until the end of image acquisition. There was a trend towards higher myocardial SUV in AL compared to ATTR amyloid patients. There was also greater variability in myocardial SUV for AL subjects than for ATTR subjects. Points on curves represent mean values for each group; error bars represent standard deviation.
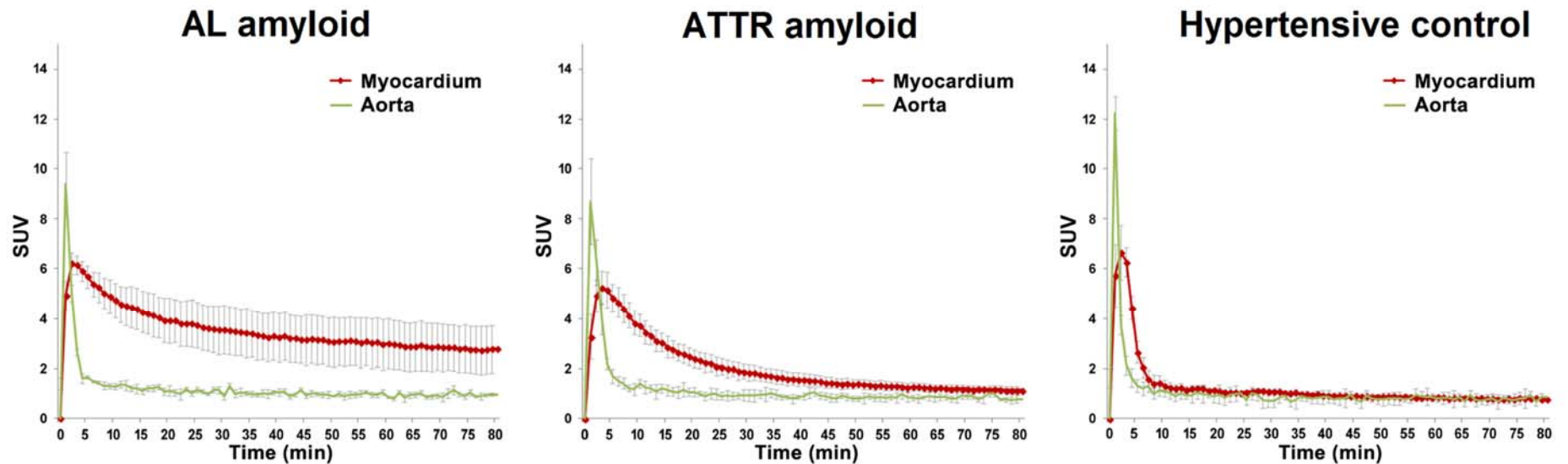
Fig. 4. ^{18}F-florbetaben RI over time in AL, ATTR and control subjects. Mean myocardial retention of ^{18}F-florbetaben was higher in both the AL and ATTR than in the control subjects. Error bars represent ranges.
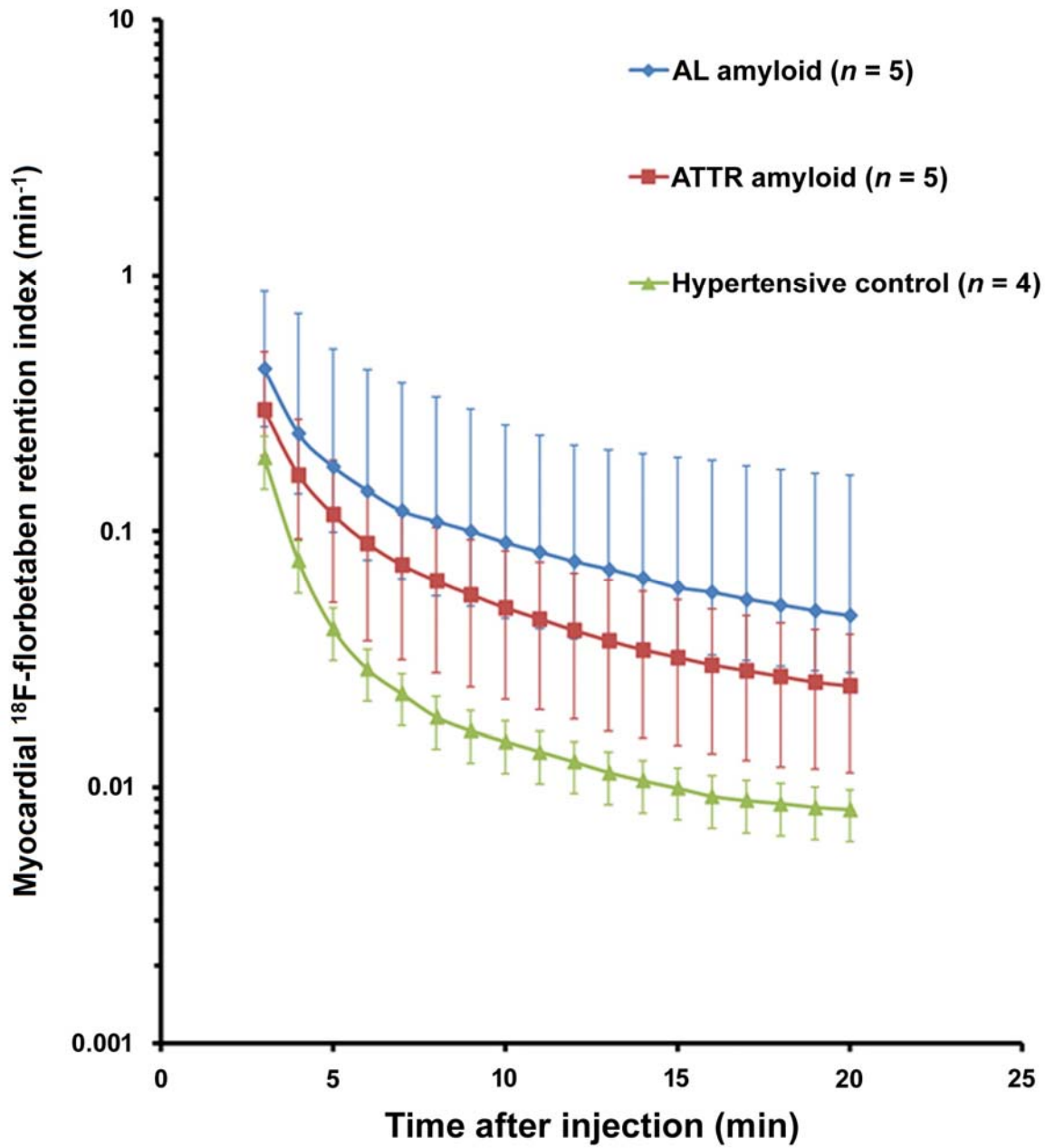
Fig. 5. Boxplots for myocardial ^{18}F-florbetaben RI for AL, ATTR and control subjects. The myocardial ^{18}F-florbetaben RI was significantly higher in AL/ATTR amyloid patients. All of the cardiac amyloid patients and none of the hypertensive control subjects had a myocardial ^{18}F-florbetaben RI >0.020min^{-1}.
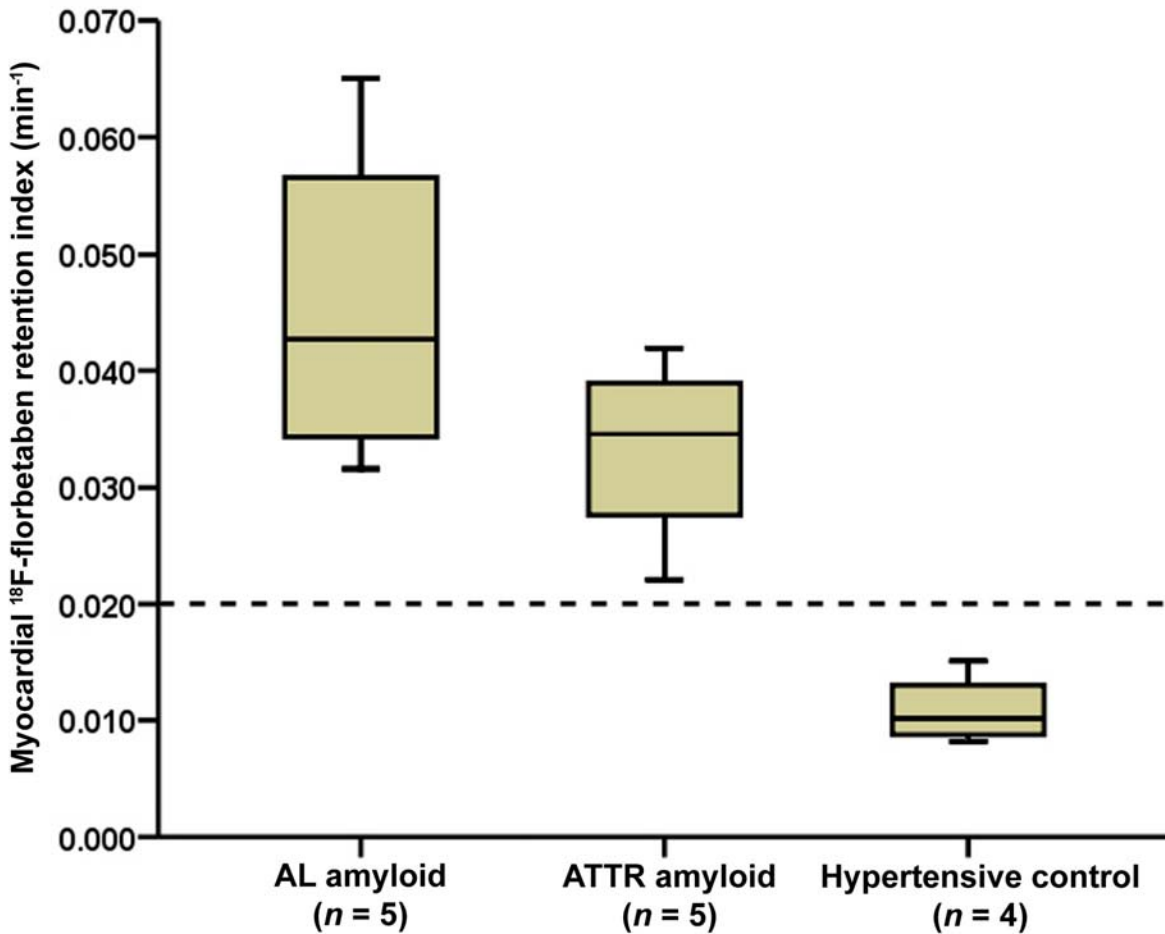
Fig. 6. Boxplots for percentage myocardial ^{18}F-florbetaben retention for AL, ATTR and control subjects. The percentage myocardial ^{18}F-florbetaben retention was significantly higher in AL/ATTR amyloid patients. All of the cardiac amyloid patients and none of the hypertensive control subjects had a myocardial retention >40%.
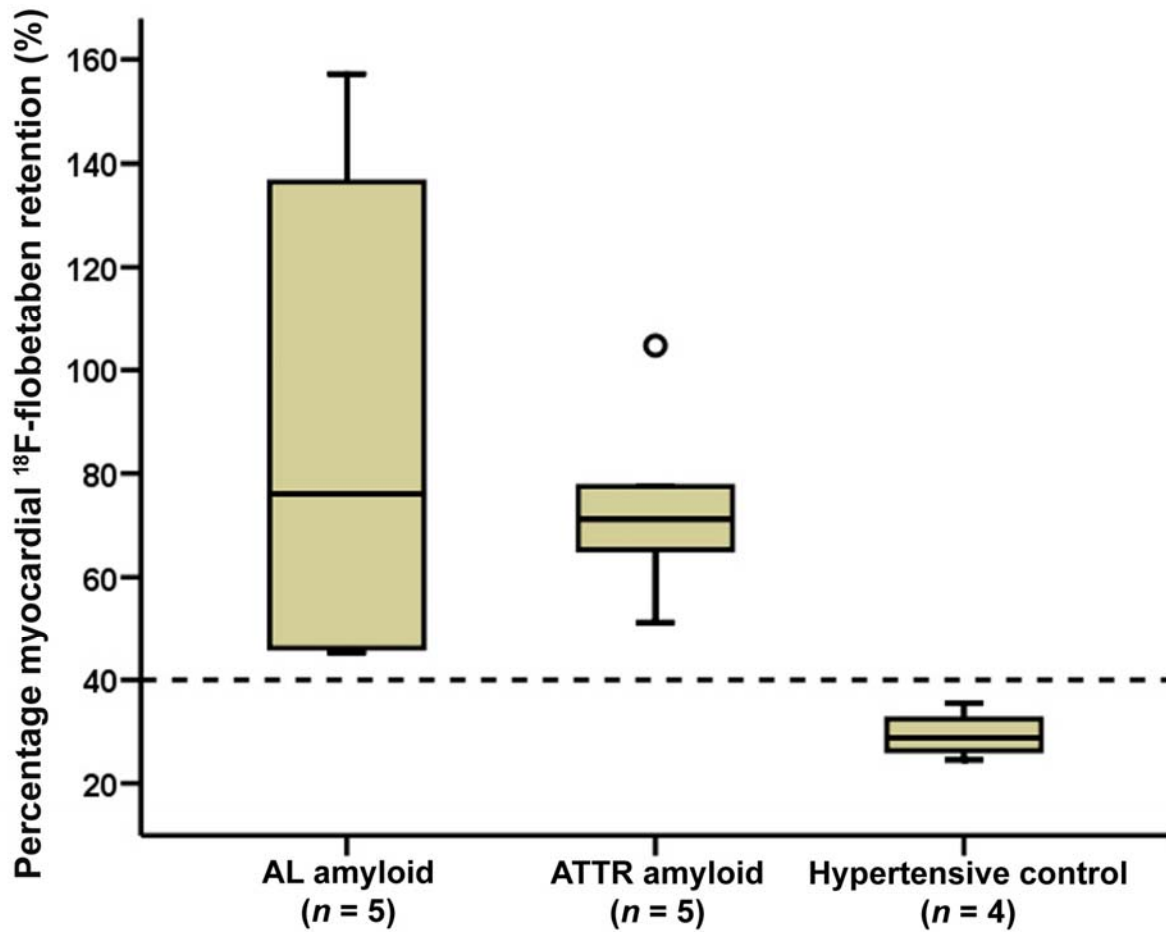
Fig. 7. Scatterplots for percentage myocardial ^{18}F-florbetaben retention versus LV global longitudinal (A) and RV free wall longitudinal strain (B), as expressed by an inverse curve relationship. Scatterplots in C and D show the inverse transformed percentage myocardial ^{18}F-florbetaben retention. Triangles indicate AL subjects, crosses indicate ATTR subjects, and circles indicate hypertensive control subjects.